

# Everything to the Synthetic: Diffusion-driven Test-time Adaptation via Synthetic-Domain Alignment

Jiayi Guo<sup>1,2</sup> Junhao Zhao<sup>1</sup> Chunjiang Ge<sup>1</sup> Chaoqun Du<sup>1</sup> Zanlin Ni<sup>1</sup> Shiji Song<sup>1</sup>  
 Humphrey Shi<sup>2†</sup> Gao Huang<sup>1†</sup>  
<sup>1</sup>Tsinghua University <sup>2</sup>SHI Labs @ Georgia Tech

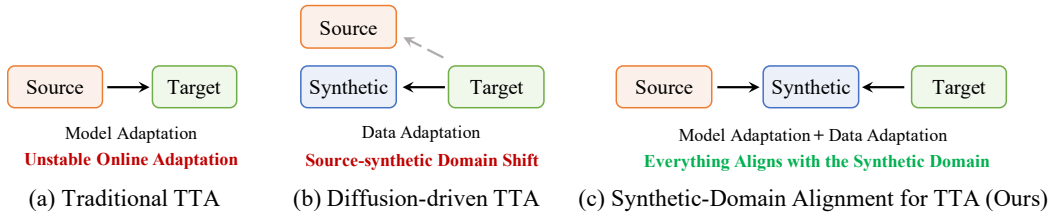


Figure 1: **Comparison of different test-time adaptation (TTA) frameworks.** (a) Traditional TTA methods adapt source model weights to fit target data. However, their performance is sensitive to the amount and order of target data streams. (b) Diffusion-driven TTA methods project the target data back to the synthetic domain of diffusion models, which still remains a gap from the source domain. (c) We propose the Synthetic-Domain Alignment framework for TTA, which simultaneously aligns the domains of the source model and target data with the synthetic domain for superior performance.

## Abstract

Test-time adaptation (TTA) aims to enhance the performance of source-domain pretrained models when tested on unknown shifted target domains. Traditional TTA methods primarily adapt model weights based on target data streams, making model performance sensitive to the amount and order of target data. Recently, diffusion-driven TTA methods have demonstrated strong performance by using an unconditional diffusion model, which is also trained on the source domain to transform target data into synthetic data as a source domain projection. This allows the source model to make predictions without weight adaptation. In this paper, we argue that the domains of the source model and the synthetic data in diffusion-driven TTA methods are not aligned. To adapt the source model to the synthetic domain of the unconditional diffusion model, we introduce a **Synthetic-Domain Alignment (SDA)** framework to fine-tune the source model with synthetic data. Specifically, we first employ a conditional diffusion model to generate labeled samples, creating a synthetic dataset. Subsequently, we use the aforementioned unconditional diffusion model to add noise to and denoise each sample before fine-tuning. This process mitigates the potential domain gap between the conditional and unconditional models. Extensive experiments across various models and benchmarks demonstrate that SDA achieves superior domain alignment and consistently outperforms existing diffusion-driven TTA methods. Our code is available at <https://github.com/SHI-Labs/Diffusion-Driven-Test-Time-Adaptation-via-Synthetic-Domain-Alignment>.

<sup>†</sup>Corresponding authors.

# 1 Introduction

Over the past decade, deep neural networks [15, 20, 7, 26, 27] have become the leading performers in various vision recognition tasks. Despite being trained on extensive datasets from source domains, these models often suffer significant performance declines when tested on shifted target-domain data [10, 19, 21, 22, 25]. These domain shifts, which are common in real-world scenarios, include image corruptions [16, 29] and adversarial attacks [24]. Consequently, deploying these source models to make predictions on shifted target data necessitates the development of effective adaptation techniques to ensure the alignment between the domains of the model and data.

Test-time adaptation (TTA) [23, 38, 47, 48, 54, 42, 9, 34, 31, 11, 46] is an emerging research area aimed at addressing domain shifts when evaluating source models on target data with unknown shifts. Generally, TTA frameworks can be categorized into two main types: 1) **Source-to-target frameworks** (Fig. 1a): These methods iteratively adapt the weights of source models to better match the target data distribution, and 2) **Target-to-source frameworks** (Fig. 1b): These approaches project target data back to their source-domain counterparts, enabling predictions within the source domain.

Traditional TTA methods (Fig. 1a) [23, 38, 47, 48, 54, 42, 9, 34] typically employ the source-to-target model adaptation framework. These approaches continuously update the weights of source models by processing batches of target data streams. Since target data lack annotations, the adaptation process relies either on updating the model’s batch-wise statistics [23, 38, 47, 48], or on conducting additional unsupervised or self-supervised auxiliary tasks [42, 9, 34]. However, target data batches may not accurately represent the true distribution of the target domain, particularly when batches are small or exhibit class imbalances. Consequently, traditional model-adaptation-based TTA methods are highly sensitive to both the amount and order of the target data stream.

Recently, the remarkable image generation capabilities of diffusion models [18, 35, 32, 52, 51, 14] have inspired a new line of diffusion-driven TTA methods (Fig. 1b) [31, 11, 46] with a target-to-source framework. These works utilize an unconditional diffusion model, which is pretrained on the source domain to project each target image back to the source domain independently. This allows the source model to make predictions without weight adaptation. In a pioneering effort, DiffPure [31] first employs diffusion models to purify adversarial target data. This technique involves initially diffusing the target data by adding a small amount of noise through a forward diffusion process, followed by restoring the clean image using a reverse diffusion process. For more challenging domain-shifted scenarios, such as images with severe corruption, subsequent studies [11, 46] enhance DiffPure by incorporating additional structural guidance from the target data to better preserve image contents.

In this paper, we argue that while diffusion-driven TTA methods aim to project target data back to the source domain, the projected target data remains confined within the synthetic domain of the unconditional diffusion model. As the data from the synthetic domain are ultimately processed by the source-domain model, the domain misalignment would limit the final performance. To address this issue, we propose **Synthetic-Domain Alignment (SDA)** ( Fig. 1c), a new category of framework for TTA tasks which *simultaneously aligns the domains of the source model and target data with the same synthetic domain of a diffusion model*.

The proposed SDA framework consists of two stages. In the first stage, we propose a supervised synthetic data fine-tuning pipeline to adapt the source model to the synthetic domain of the unconditional diffusion model used in diffusion-driven TTA methods. Specifically, we first employ a conditional diffusion model to generate samples using domain-agnostic labels as conditions, creating a labeled synthetic dataset. Subsequently, we use the aforementioned unconditional diffusion model to add noise to and denoise each sample before fine-tuning. This process mitigates the potential domain gap between the conditional and unconditional models. With a sufficiently large synthetic dataset, the fine-tuned model becomes highly discriminative to synthetic-domain data. In the second stage, we use diffusion-driven TTA methods to project target data into the synthetic domain. Therefore, the proposed SDA framework effectively transforms the cross-domain TTA task into an in-domain prediction task, as both the domains of the source model and target data are aligned with the same synthetic domain. It is worth noting that the main contribution of SDA is proposing a general TTA framework from the synthetic-domain alignment perspective. Consequently, the framework is not tied to specific source model fine-tuning techniques or diffusion-driven target data adaptation methods. As these techniques evolve, they will further enhance the performance and broaden the applicability of SDA. Extensive experiments across various model architectures and benchmarks demonstrate that

SDA outperforms existing diffusion-driven TTA methods. Moreover, our results are supported by visualization analysis and ablation studies, further validating the effectiveness of SDA.

## 2 Related Work

**Test-time adaptation (TTA)** is an emerging research topic to deal with domain shifts by either model adaptation [23, 38, 47, 48, 54, 42, 9, 34] or data adaptation [31, 11, 46] when evaluating source-domain models on shifted target data. For model adaptation TTA methods, earlier works update batch normalization statistics of the source model to fit the target distribution [23, 38]. TENT [47] learns to adjust model weights by minimizing test-time prediction entropy. MEMO [54] minimizes the marginal entropy between input data and its augmented views to adapt the model. Another line of work also investigates leveraging self-supervised auxiliary tasks to update model weights, such as rotation prediction [42] and image restoration [9, 34]. However, most model adaptation TTA methods rely on continuous model weight updates via test-time target data streams and thus can be sensitive to the amount, order, and diversity of the target data. Recently, diffusion-driven TTA methods propose the data adaptation framework [31, 11, 46] to independently project each target data back to the source domain. Without the need for online model adaptation, these methods showcase stable performance. DiffPure [31] first proposes to purify the adversarial samples with diffusion models. DDA [11] and GDA [46] introduce additional structural guidance to preserve image content under severe corruption. As aforementioned, our work aims to mitigate the gap between the domains of diffusion synthetic images and the source model in diffusion-driven TTA methods using a new synthetic-domain alignment TTA framework.

**Synthetic data for discriminative tasks.** Synthetic data is fully or partly synthesized by generative models rather than being collected from the real world. Learning from synthetic data [43, 13, 44, 8] has been proven to be effective in enhancing the visual representation in various discriminative tasks, including visual recognition [2, 44], object detection [37, 33], semantic segmentation [36, 3, 40], image assessment [12], autonomous driving [1] and robotics [30, 53]. For instance, Azizi *et al.* [2] demonstrate that combining the real data from ImageNet [5] and synthetic data from a fine-tuned Imagen [39] diffusion model improves classification accuracy. DA-Fusion [45] augments the semantic attributes of training data with diffusion models to enhance the generalization capabilities. StabeRep [44] utilizes synthetic images generated by Stable Diffusion [35] to construct stronger visual representation learners. In this work, we focus on investigating the potential of domain alignment in TTA tasks using synthetic data generated by diffusion models.

## 3 Preliminaries

### 3.1 Diffusion-based Image Generation

Diffusion models have recently achieved state-of-the-art performance in image generation tasks. In essence, these models involve a forward process transforming an image into noise and a reverse process turning a noise into an image. Specifically, the forward process is a Markov chain that gradually adds random Gaussian noise  $\epsilon_t \sim N(\mathbf{0}, \mathbf{I})$  to an image sampled from the real data distribution  $\mathbf{x}_0 \sim p(\mathbf{x}_0)$ , over a total of  $T$  steps. At each step  $t$ , the noisy data  $\mathbf{x}_t$  is computed as:

$$\mathbf{x}_t = \sqrt{1 - \beta_t} \mathbf{x}_{t-1} + \sqrt{\beta_t} \epsilon_t, \quad t = 1, 2, \dots, T, \quad (1)$$

where  $\beta_t \in (0, 1)$  is the preset diffusion rate at step  $t$ . By setting  $\alpha_t = 1 - \beta_t$ ,  $\bar{\alpha}_t = \prod_{s=1}^t \alpha_s$  and  $\epsilon \sim N(\mathbf{0}, \mathbf{I})$ , we have the following equivalents:

$$\mathbf{x}_t = \sqrt{\alpha_t} \mathbf{x}_{t-1} + \sqrt{1 - \alpha_t} \epsilon_t = \sqrt{\bar{\alpha}_t} \mathbf{x}_0 + \sqrt{1 - \bar{\alpha}_t} \epsilon, \quad t = 1, 2, \dots, T. \quad (2)$$

Note that as  $T$  becomes sufficiently large,  $\bar{\alpha}_t$  tends towards zero. Thus  $\mathbf{x}_T$  is close to  $\epsilon \sim N(\mathbf{0}, \mathbf{I})$ .

Given the noisy data  $\mathbf{x}_t$  as input, along with the time step  $t$  and an optional condition  $y$  for conditional diffusion models, a diffusion model  $\epsilon_\phi$  is trained to predict the noise component  $\epsilon$ . A prevalent training objective utilized in modern diffusion models [18, 35] is:

$$\mathcal{L} = \mathbb{E}_{\mathbf{x}_0, \epsilon, t, c} \|\epsilon - \epsilon_\phi(\mathbf{x}_t, t, y)\|_2^2. \quad (3)$$

After diffusion training, the reverse diffusion process is able to synthesize a sequence of denoised images  $\{\mathbf{x}_{T-1}^{\text{syn}}, \mathbf{x}_{T-2}^{\text{syn}}, \dots, \mathbf{x}_0^{\text{syn}}\}$  by gradually removing noise from a degraded  $\mathbf{x}_T$ :

$$\mathbf{x}_{t-1}^{\text{syn}} = \frac{1}{\sqrt{\alpha_t}} \left( \mathbf{x}_t^{\text{syn}} - \frac{1 - \alpha_t}{\sqrt{1 - \alpha_t}} \epsilon_\phi(\mathbf{x}_t^{\text{syn}}, t, y) \right) + \sigma_t \epsilon, \quad t = 1, 2, \dots, T, \quad (4)$$

where  $\sigma_t$  is the posterior noise variance [18] determined by  $\{\beta_t\}_{t=0}^T$ .

### 3.2 Revisiting Existing Test-time Adaptation Frameworks

In the classical visual recognition setting, we are given a model  $f_\theta$  with parameters  $\theta$ , which is trained on specific source domain data  $\mathbf{x}_0^{\text{src}} \sim p(\mathbf{x}_0^{\text{src}})$ . For an input  $\mathbf{x}_0^{\text{src}}$ , the model  $f_\theta$  produce a conditional output distribution  $p_\theta(y|\mathbf{x}_0^{\text{src}})$  and the predicted label  $\hat{y} = \arg \max_y p_\theta(y|\mathbf{x}_0^{\text{src}})$  is usually accurate. However, when evaluated on shifted target-domain data  $\mathbf{x}_0^{\text{trg}} \sim p(\mathbf{x}_0^{\text{trg}})$ , the source model  $f_\theta$  often encounters significant performance degradation due to the domain shift.

Test-time adaptation (TTA) is the process of improving the performance of model  $f_\theta$  on target data  $\mathbf{x}_0^{\text{trg}}$  from various unknown domains. Existing TTA frameworks can be categorized into two main types: (1) source-to-target frameworks, which adapt parameters  $\theta$  of  $f_\theta$  to fit the target data distribution  $p(\mathbf{x}_0^{\text{trg}})$  and (2) target-to-source frameworks, which project target data  $\mathbf{x}_0^{\text{trg}}$  back to its source-domain counterpart  $\mathbf{x}_0^{\text{src}}$ . In this section, we revisit the potential shortcomings of these existing frameworks that motivate the development of our proposed SDA framework in Sec. 4.

**Source-to-target frameworks.** Traditional TTA methods primarily employ an online model adaptation paradigm, where methods like adjusting batch normalization statistics [23, 38, 47, 48] or updating model weights through self-supervised auxiliary tasks [42, 9, 34] are applied to  $f_\theta$  using batched test-time target data  $\mathbf{x}_0^{\text{trg}}$ . Ideally, these adaptations transform  $f_\theta$  into a discriminative model for the target domain,  $f_{\theta'}$ . However, real-world scenarios often present challenges such as insufficient or class-imbalanced test data batches, leading to suboptimal model adaptation. These issues may result in  $f_{\theta'}$  overfitting specific classes and delivering inaccurate predictions.

**Target-to-source frameworks.** Recent advancements in diffusion models for image generation have inspired diffusion-driven TTA methods [31, 11, 46]. These approaches adopt a data adaptation paradigm, utilizing a source-domain pretrained unconditional diffusion model,  $\epsilon_\phi^u$ , to independently re-synthesize each sample in target data  $\mathbf{x}_0^{\text{trg}}$ . The underlying hypothesis is that the discrepancies between the source data  $\mathbf{x}_0^{\text{src}}$  and its domain-shifted target counterpart  $\mathbf{x}_0^{\text{trg}}$  can be progressively reduced by the diffusion forward process (Eq. 2) as the timestep  $t$  increases [31]. Ideally, at a sufficiently large  $t$ ,  $\mathbf{x}_t^{\text{trg}}$  will closely approximate  $\mathbf{x}_t^{\text{src}}$ . Through the diffusion reverse process (Eq. 4), diffusion-driven TTA methods then project  $\mathbf{x}_t^{\text{trg}}$  back to  $\mathbf{x}_0^{\text{syn}}$ , which acts as an estimate of  $\mathbf{x}_0^{\text{src}}$  within the synthetic domain of  $\epsilon_\phi^u$ . Predictions are finally made based on  $p_\theta(y|\mathbf{x}_0^{\text{syn}})$ .

Although diffusion-driven TTA methods avoid the unstable online adaptation required by traditional TTA methods, the synthetic data  $\mathbf{x}_0^{\text{syn}}$  cannot perfectly emulate  $\mathbf{x}_0^{\text{src}}$  due to the imperfect distribution modeling capabilities of generative models [49, 50]. This inherent domain gap between  $\mathbf{x}_0^{\text{syn}}$  and  $\mathbf{x}_0^{\text{src}}$  can hinder the performance of  $f_\theta$ , impacting the accuracy and reliability of predictions.

## 4 Synthetic-domain Alignment Framework for Test-time Adaptation.

The aforementioned limitations of existing TTA frameworks demonstrate that achieving direct ‘‘source-to-target’’ or ‘‘target-to-source’’ domain adaptation is not straightforward. This raises the question: Can we identify an intermediary domain where both the source model  $f_\theta$  and target data  $\mathbf{x}_0^{\text{trg}}$  can be more effectively adapted? In this section, we argue that the synthetic domain, constructed by synthetic data generated through a diffusion model, serves as an ideal intermediary domain.

As depicted in Fig. 2, we propose **Synthetic-Domain Alignment (SDA)**, a novel TTA framework that simultaneously aligns the domains of the source model  $f_\theta$  and target data  $\mathbf{x}_0^{\text{trg}}$  with the synthetic domain of an unconditional diffusion model. SDA framework comprises two stages. In Stage 1, we introduce a synthetic data fine-tuning pipeline to adapt the source model  $f_\theta$  to a synthetic-domain model  $f_{\theta'}$ . In specific, the data fine-tuning pipeline further involves (1) utilizing a conditional diffusion model  $\epsilon_\eta^c$  to construct a labeled synthetic dataset for fine-tuning and (2) aligning the domain

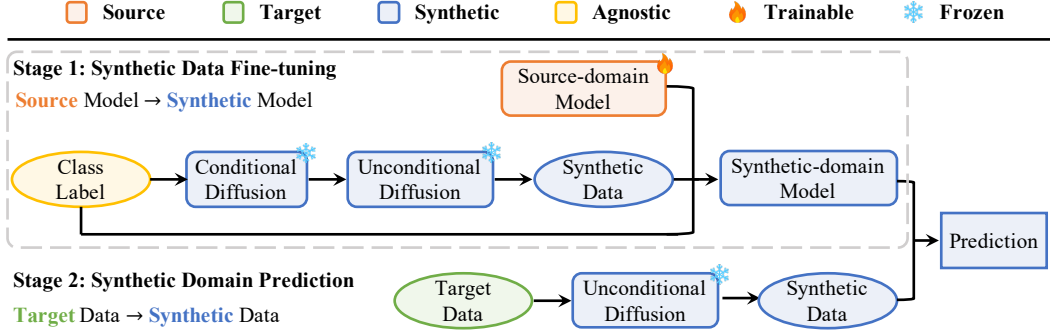


Figure 2: **Overview of the Synthetic-Domain Alignment (SDA) framework.** SDA is a novel two-stage TTA framework aligning both the domains of the source model and the target data with the synthetic domain. In Stage 1, the source-domain model is adapted to a synthetic-domain model through synthetic data fine-tuning. This synthetic data is first generated using a conditional diffusion model based on domain-agnostic class labels, then re-synthesized through an unconditional diffusion process to ensure domain alignment with the projected target data in Stage 2. In Stage 2, target data is projected into the synthetic domain using unconditional diffusion. The final prediction is produced by processing the synthetic data through the adapted synthetic-domain model.

of the dataset with the synthetic domain of an unconditional diffusion model  $\epsilon_\phi^u$ . In Stage 2, we follow the diffusion-driven TTA methods to project target data  $\mathbf{x}_0^{\text{trg}}$  back to its synthetic-domain counterpart  $\mathbf{x}_0^{\text{syn}}$  via  $\epsilon_\phi^u$ . Finally, the domains of the model  $f_{\theta'}$  and data  $\mathbf{x}_0^{\text{syn}}$  are aligned with the same synthetic domain of  $\epsilon_\phi^u$ . Since the domain gap is mitigated, the model performance is naturally to be enhanced.

#### 4.1 Construct a Labeled Synthetic Dataset via Conditional Diffusion.

In the context of TTA, despite the existing domain shift, the source and target domains are expected to share the same set of domain-agnostic prediction labels. For instance, in TTA classification tasks, the  $K$  class labels  $\{y_i\}_{i=1}^K$  are known prior to testing. Utilizing a powerful source-domain conditional diffusion model,  $\epsilon_\eta^c$ , with parameters  $\eta$ , we can uniformly generate  $N$  samples for each class  $y_i$  from random Gaussian noise through the  $T$ -step reverse diffusion process (Eq. 4). The generation capability of diffusion models allows for the construction of an arbitrary large labeled synthetic-domain dataset  $\{\mathbf{x}_{0,c}^{\text{syn}}, y\}^{K \times N}$  without the need for manual data collection. By fine-tuning the source model  $f_\theta$  on this synthetic dataset, a synthetic-domain model  $f_{\theta'}$  can be obtained.

#### 4.2 Align Synthetic Data via Unconditional Diffusion

Given that the diffusion-driven TTA method in Stage 2 employs an unconditional diffusion model,  $\epsilon_\phi^u$ , with parameters  $\phi$  to project target data to the synthetic domain of  $\epsilon_\phi^u$ , there is a potential domain gap between the synthetic domains of the unconditional  $\epsilon_\phi^u$  and the conditional  $\epsilon_\eta^c$ . This gap primarily arises due to different training loss functions (Eq. 3) and model architectures between  $\epsilon_\phi^u$  and  $\epsilon_\eta^c$ . To address this challenge, we employ  $\epsilon_\phi^u$  to align the synthetic data  $\mathbf{x}_{0,c}^{\text{syn}}$  generated by  $\epsilon_\eta^c$  before initiating source model fine-tuning. This alignment process mirrors the diffusion-driven target data adaptation method: Standard Gaussian noise is first added to  $\mathbf{x}_{0,c}^{\text{syn}}$  according to a specific timestep  $t$ , creating the noisy  $\mathbf{x}_{t,c}^{\text{syn}}$  via the forward diffusion process (Eq. 2). Subsequently, using the reverse diffusion process (Eq. 4), the  $\mathbf{x}_{t,c}^{\text{syn}}$  is recovered to a clean  $\mathbf{x}_{0,u}^{\text{syn}}$  by  $\epsilon_\phi^u$ . The alignment ensures that both the synthetic data used for model fine-tuning in Stage 1 and for model prediction in Stage 2 are projected to the same synthetic domain of  $\epsilon_\phi^u$ .

#### 4.3 Overall Process

The overall process of SDA for TTA tasks is as follows. First, we construct a labeled synthetic dataset using both conditional diffusion  $\epsilon_\eta^c$  and unconditional diffusion  $\epsilon_\phi^u$ . Then, through supervised fine-tuning on the labeled synthetic dataset, the source-domain model  $f_\theta$  is adapted to a synthetic-domain

model  $f_{\theta'}$ . Next, assisted with diffusion-driven TTA methods, *e.g.*, DDA [11], target data  $\mathbf{x}_0^{\text{trg}}$  is projected to their synthetic-domain counterpart  $\mathbf{x}_0^{\text{syn}}$ . Consistent with the protocol of DDA, the final prediction is an ensemble of the model predictions of  $\mathbf{x}_0^{\text{trg}}$  and  $\mathbf{x}_0^{\text{syn}}$ . We differentiate SDA from DDA by using synthetic-domain model  $f_{\theta'}$  to predict on  $\mathbf{x}_0^{\text{syn}}$ :

$$\hat{y} = \arg \max_y (p_{\theta}(y|\mathbf{x}_0^{\text{trg}}) + p_{\theta'}(y|\mathbf{x}_0^{\text{syn}})), \quad (5)$$

where  $p_{\theta}(\cdot)$  and  $p_{\theta'}(\cdot)$  are predicted output distributions by the model  $f_{\theta}$  and  $f_{\theta'}$ , respectively.

## 5 Experiments

### 5.1 Experimental Setup

**Baselines.** We choose DDA [11] as our primary competitor since it is the best-performing publicly available diffusion-driven TTA method. Following DDA, we include the early DiffPure [31] and the single-sample model adaptation method MEMO [54] as baselines. Additionally, we compare SDA against the recent SOTA diffusion-driven TTA method, GDA [46] based on their paper results. The performance of source models without any adaptation is reported as the "Source" setting.

**Models.** For source-domain models, we explore both CNN and Transformer classifiers, including ResNet50 [15], ConvNeXt [27], and Swin Transformers [26]. For the unconditional diffusion model, we select the same ADM [6] as baselines. For the conditional diffusion model, we select the popular Diffusion Transformer (DiT) [32]. All models are trained on ImageNet [5] before deployment.

**Datasets.** We evaluate our SDA framework on ImageNet-C [16] and ImageNet-W [24]. ImageNet-C [16] is a standard robust image classification benchmark. It contains 15 different corruption types in 4 categories: noise, blur, weather and digital artifacts. Each corruption type further consists of 5 severity levels, with 50000 images per level. Our tests are conducted on the most severe level 5. ImageNet-W [24] is another recent robust benchmark, containing 50000 images with watermark artifacts. We construct the ImageNet-W dataset based on the official code.

**Implementation details.** All our experiments are conducted with  $8 \times$  A100 80G GPUs. For synthetic dataset generation with conditional diffusion, we adopt DiT-XL/2 ( $256 \times 256$ ) [32] to generate 50000 samples, with 50 samples for each of the 1000 ImageNet classes. The number of sampling steps is set to 250, and the classifier-free guidance is set to 1.0. The generation period takes about 3 hours. For data alignment with unconditional diffusion, ADM [6] is employed with 100 diffusion steps. Following DDA [11], we add noise and denoise over 50 steps with structural guidance. The alignment period requires about 6 hours. For synthetic data fine-tuning, each classifier is fine-tuned for 15 epochs. We use Stochastic Gradient Descent (SGD) with a learning rate of  $5e-4$  and a batch size of 512 for ResNet and AdamW optimizer [28] with a learning rate of  $2e-5$  and a batch size of 1024 for ConvNeXt [27] and Swin [26]. The fine-tuning period requires less than 10 minutes. We employ DDA [11] to project target images to the synthetic domain in the second stage of SDA.

Table 1: **Quantitative evaluations on ImageNet-C [16].** We compare SDA with source models without adaptation, MEMO [54], DiffPure [31], GDA [46] and DDA [11]. Results are reported using the average accuracy across 15 corruption types at severity level 5. The best results are in bold.

Model	Source	MEMO	DiffPure	GDA	DDA	SDA (Ours)
ResNet-50	18.7	24.7	16.8	31.8	29.7	<b>32.5 (+2.8)</b>
Swin-T	33.1	29.5	24.8	42.2	40.0	<b>42.5 (+2.5)</b>
ConvNeXt-T	39.3	37.8	28.8	44.8	44.2	<b>47.0 (+2.8)</b>
Swin-B	40.5	37.0	28.9	-	44.5	<b>47.4 (+2.9)</b>
ConvNeXt-B	45.6	45.8	32.7	-	49.4	<b>51.9 (+2.5)</b>

### 5.2 Empirical Results

**Qualitative evaluations on ImageNet-C.** We begin by evaluating the performance of SDA on ImageNet-C. As reported in Tab. 1, our proposed SDA consistently outperforms all baseline methods across different model architectures and sizes. We emphasize the performance improvement over DDA, as we adopted DDA to project target data to the synthetic domain in Stage 2 of SDA. Compared to DDA, our SDA improves accuracy by 2.5%-2.9%. This significant improvement indicates the

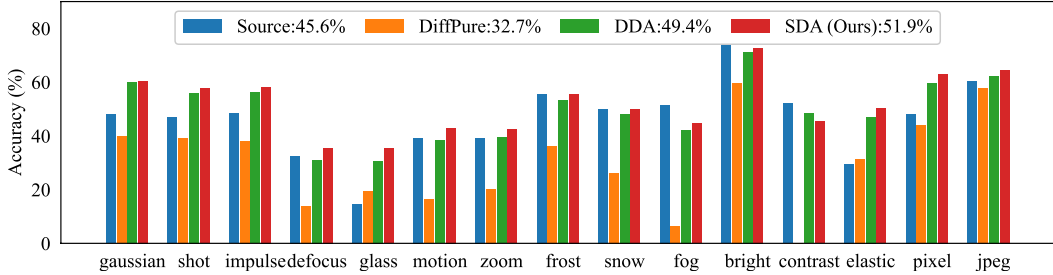


Figure 3: **Detailed comparisons of SDA and baselines across 15 corruption types on ImageNet-C.** SDA surpasses baselines for most corruption types and shows the best average accuracy. The results are obtained using ConvNeXt-B. Comparisons with other classifiers are deferred to the appendix.

misalignment between the source and synthetic domains, validating the effectiveness of our synthetic-domain alignment framework. Moreover, compared to the recent SOTA GDA, SDA also achieves an improvement of 2.2% with ConvNeXt-T. Notably, SDA focuses on synthetic domain alignment, an orthogonal research direction to existing efforts on better de-corrupting the target data. Therefore, the performance of SDA could potentially be further enhanced with the release of more advanced codebases like GDA. Compared to the model adaptation method MEMO, three diffusion-driven methods (SDA, DDA, and GDA) all demonstrate superior performance, highlighting the effectiveness of diffusion models in assisting TTA tasks. DiffPure presents worse results since it is primarily designed for adversarial attacks. Without the structural guidance introduced in DDA and GDA, DiffPure may not effectively recover images with severe corruption.

In Fig. 3, we provide a detailed comparison of the results of SDA and baselines. SDA outperforms DiffPure in all 15 corruption types and surpasses DDA in 14 out of 15 corruption types, affirming its effectiveness across various domain shifts. The sole exception is under the contrast corruption type, where SDA’s performance decline may be attributed to DDA’s inferior performance compared to the source model in this specific corruption type. This suggests that after DDA’s de-corruption process, the synthetic images become less discriminative compared to the original target images, potentially enlarging the domain shift. As SDA fine-tunes source models to fit the synthetic domain but not the target domains, its performance can be adversely impacted when diffusion models inadequately de-corrupt the target data.

**Qualitative results on ImageNet-W.** We extend our evaluations to include ImageNet-W to test the performance of SDA against watermark-based domain shifts. As shown in Tab. 2, SDA consistently outperforms all baselines across various models. Notably, SDA achieves accuracy improvements ranging from 1.4% to 2.3% over our core baseline DDA, underscoring the effectiveness of

Table 2: **Quantitative results on ImageNet-W [24].** The best results are in bold.

Model	Source	DiffPure	DDA	SDA (Ours)
ResNet-50	37.7	29.1	52.8	<b>54.7 (+1.9)</b>
Swin-T	66.5	52.7	65.9	<b>67.3 (+1.4)</b>
ConvNeXt-T	67.6	55.8	67.9	<b>69.4 (+1.5)</b>
Swin-B	69.1	55.5	68.3	<b>70.6 (+2.3)</b>
ConvNeXt-B	70.1	57.7	70.3	<b>72.3 (+2.0)</b>

synthetic-domain alignment under watermark artifacts. Similar to the findings in Fig. 3, Tab. 2 also indicates potential performance declines when DDA is applied to ImageNet-W with Swin-T and Swin-B models, suggesting that diffusion re-synthesized images may not always enhance model accuracy. Nonetheless, the consistent improvements of SDA further suggest that it points out an insightful performance-improving direction for diffusion-driven TTA methods.

### 5.3 Analysis

**Visualization.** To illustrate how synthetic data fine-tuning in SDA enhances the performance of diffusion-driven TTA methods, we employ Gradient-weighted Class Activation Mapping (Grad-CAM) [41]. This technique visualizes the image regions most influential to the classification scores across different images and models. As shown in Fig. 4, testing target images with the source model reveals differences in activation maps and the occurrence of incorrect predictions compared to those from source images, underscoring the performance degradation due to domain shifts. Despite using de-corrupted synthetic images, DDA still risks focusing on inappropriate regions and producing incorrect predictions. This highlights the domain misalignment of the synthetic data and source model.

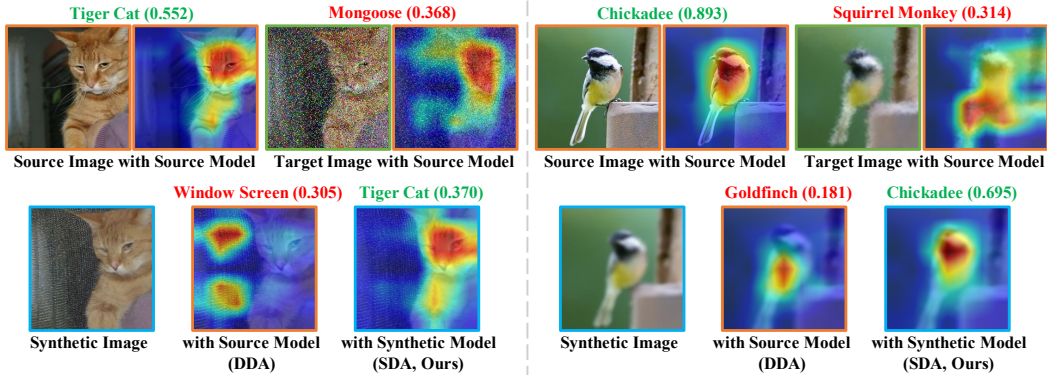


Figure 4: **Gradient-weighted Class Activation Mapping (Grad-CAM) Visualization Comparison.** The first row shows activation maps when evaluating *source* and *target* domain images using the *source* model. The second row presents activation maps when evaluating diffusion *synthetic* images using the *source* model (DDA) and our *synthetic*-domain model (SDA). The corresponding prediction classes and confidence scores are displayed above the images. Our SDA achieves alignment within the synthetic domain and, therefore, showcases activation maps and prediction results that aligns more closely with those from the “source image with source model!” scenario. The visualization results are conducted using Swin-T with corruption types impulse noise (left) and glass blur (right).

In contrast, SDA achieves synthetic-domain alignment of the data and model, thereby producing activation maps and predictions that closely match the "source image with source model" scenario.

**Time cost.** While SDA incurs additional time for generating synthetic data and fine-tuning source models compared to existing diffusion-driven TTA methods, this process can be integrated as part of an extended two-stage pretraining routine. The initial phase involves pretraining in the source domain, followed by fine-tuning in the synthetic domain. Synthetic data generation is required only once and is applicable across different models. This generation can be executed in parallel with source-domain pretraining. For synthetic-domain fine-tuning, empirical results in Tab. 3 indicate that the fine-tuning phase of synthetic data consumes less than 0.6% of the source-domain pretraining time, showcasing its efficiency.

Table 3: **Time comparisons (hours) of source model pretraining and SDA fine-tuning (SDA-FT).** Experiments are conducted with  $8 \times$  A100 GPUs.

Model	Pretraining	SDA-FT
ResNet-50	6.9	0.04
Swin-T	25.1	0.05
ConvNeXt-T	32.8	0.07
Swin-B	54.7	0.10
ConvNeXt-B	64.3	0.13

## 5.4 Ablation Studies

**Components.** We analyze the impact of two key components in our SDA framework’s synthetic data fine-tuning process, as detailed in Tab. 4: (1) synthetic data generation via the conditional diffusion model (introduced in Sec. 4.1), and (2) synthetic data alignment via the unconditional diffusion model (depicted in Sec. 4.2). Using synthetic data generated by the conditional diffusion model alone (+ Conditional Data Synthesis) to fine-tune source models typically results in marginal improvements and may even lead to performance degradation. Notably, when the synthetic data is further aligned through the unconditional diffusion model (+ Unconditional Alignment), the fine-tuned model consistently outperforms the baseline DDA. This significant improvement underscores the domain gap between the synthetic data of different diffusion models. Our proposed synthetic data alignment process effectively bridges this gap, proving crucial for the success of our SDA framework.

**Number of fine-tuning images.** We analyze the impact of different numbers of images ( $N$ ) used during the synthetic data fine-tuning process, as detailed in Tab. 5. Interestingly, even with only one image per class ( $N = 1k$ ), SDA still significantly outperforms DDA. This finding suggests a key attribute of the fine-tuning process: source models are primarily learning to adapt to the synthetic domain itself, rather than acquiring class-specific knowledge. Increasing the number of images helps the fine-tuning process capture the synthetic domain more accurately, thereby enhancing performance.



Table 4: **Ablation results of different components in SDA.** The best results are in bold.

Component	ImageNet-C			ImageNet-W		
	ResNet-50	Swin-T	ConvNeXt-T	ResNet-50	Swin-T	ConvNeXt-T
DDA [11]	29.7	40.0	44.2	52.8	65.9	67.9
+ Conditional Data Synthesis	30.4	39.2	44.2	52.3	65.3	67.7
+ Unconditional Alignment	<b>32.5</b>	<b>42.5</b>	<b>47.0</b>	<b>54.7</b>	<b>67.3</b>	<b>69.4</b>

Based on a balance between performance improvement and the time cost of generating images, we select N = 50k as our default experimental setting.

Table 5: **Ablation results of different numbers of fine-tuning images.** The best results are in bold.

Method	Number (N)	ImageNet-C			ImageNet-W		
		ResNet-50	Swin-T	ConvNeXt-T	ResNet-50	Swin-T	ConvNeXt-T
DDA [11]	0	29.7	40.0	44.2	52.8	65.9	67.9
SDA	1k	31.9	42.3	45.5	53.7	66.7	68.6
	10k	31.9	<b>42.5</b>	46.6	54.4	67.2	69.0
	50k (default)	32.5	<b>42.5</b>	<b>47.0</b>	<b>54.7</b>	67.3	<b>69.4</b>
	100k	<b>32.6</b>	42.2	46.8	54.6	<b>67.5</b>	<b>69.4</b>

**Classifier-free guidance scale for conditional diffusion.** We analyze the impact of varying classifier-free guidance (CFG) scales on the conditional DiT [32] model, as detailed in Tab. 6. CFG is a technique employed in conditional diffusion models to manage the trade-off between synthetic image quality and diversity. A higher CFG scale typically improves image quality but may compromise diversity. We test CFG scales of {1, 1.5, 4.0}, which correspond to the basic conditional generation scale, the optimal scale for Fréchet Inception Distance (FID) [17], and the best scale for visual quality according to the DiT’s original paper [32], respectively. Our empirical results indicate that a CFG of 1 maintains consistent performance across all models and datasets. Conversely, increasing the CFG scale can potentially degrade performance, likely due to reduced image diversity.

Table 6: **Ablation results of different classifier-free guidance scales.** The best results are in bold.

Classifier-free guidance (CFG)	ImageNet-C			ImageNet-W		
	ResNet-50	Swin-T	ConvNeXt-T	ResNet-50	Swin-T	ConvNeXt-T
1.0 (default)	<b>32.5</b>	<b>42.5</b>	<b>47.0</b>	<b>54.7</b>	<b>67.3</b>	<b>69.4</b>
1.5	32.0	41.6	46.0	<b>54.7</b>	67.1	69.0
4.0	30.1	38.5	42.4	54.0	66.3	68.4

## 6 Discussion

**Limitations.** SDA employs diffusion models for synthetic data generation and alignment, inheriting the low test speed characteristic of existing diffusion-driven TTA methods [31, 11, 46]. It can be improved by developing faster diffusion samplers and distillation techniques. Additionally, SDA requires an extra fine-tuning process to adapt the source model to the synthetic domain, introducing more time overhead. However, as demonstrated in Tab. 3, the increase in fine-tuning time is extremely marginal when compared to the extensive source-model pretraining. Given the significant performance improvements, this modest increment in training time should be considered acceptable.

**Boarder Impact.** The quality of synthetic data depends on the generation capabilities of the diffusion models. While synthetic data can effectively mimic realistic data, it may not fully capture some crucial attributes for specific tasks. However, future advancements in diffusion models are expected to improve this aspect significantly. The core innovation of SDA lies in introducing and validating a novel framework for domain adaptation within the synthetic domain. This approach is anticipated to pave the way for future research in the border field of synthetic data-based learning paradigms.

## 7 Conclusion

In this paper, we proposed **Synthetic-Domain Alignment (SDA)**, a novel test-time adaptation (TTA) framework that simultaneously aligns the domains of the source model and target data with the synthetic domain of a diffusion model. For the source model, SDA adopts a synthetic data fine-tuning pipeline to adapt it to a synthetic domain model. This pipeline involves a conditional diffusion model for synthetic data generation and an unconditional diffusion model for synthetic data alignment. For the target data, SDA leverages the aforementioned unconditional diffusion model to project the target data to the synthetic data. As the domains of the model and data are aligned, SDA successfully converts the cross-domain TTA task into an easier in-domain prediction task. Extensive experiments across various models and benchmarks demonstrate that SDA achieves superior domain alignment and consistently outperforms existing diffusion-driven TTA methods.

## References

- [1] Hassan Abu Alhaija, Siva Karthik Mustikovela, Lars Mescheder, Andreas Geiger, and Carsten Rother. Augmented reality meets computer vision: Efficient data generation for urban driving scenes. *IJCV*, 2018.
- [2] Shekoofeh Azizi, Simon Kornblith, Chitwan Saharia, Mohammad Norouzi, and David J. Fleet. Synthetic data from diffusion models improves imagenet classification. *TMLR*, 2023.
- [3] Yuhua Chen, Wen Li, Xiaoran Chen, and Luc Van Gool. Learning semantic segmentation from synthetic data: A geometrically guided input-output adaptation approach. In *CVPR*, 2019.
- [4] MMPreTrain Contributors. Openmmlab’s pre-training toolbox and benchmark. <https://github.com/open-mmlab/mmpretrain>, 2023.
- [5] Jia Deng, Wei Dong, Richard Socher, Li-Jia Li, Kai Li, and Li Fei-Fei. Imagenet: A large-scale hierarchical image database. In *CVPR*, 2009.
- [6] Prafulla Dhariwal and Alexander Nichol. Diffusion models beat gans on image synthesis. In *NeurIPS*, 2021.
- [7] Alexey Dosovitskiy, Lucas Beyer, Alexander Kolesnikov, Dirk Weissenborn, Xiaohua Zhai, Thomas Unterthiner, Mostafa Dehghani, Matthias Minderer, Georg Heigold, Sylvain Gelly, et al. An image is worth 16x16 words: Transformers for image recognition at scale. In *ICLR*, 2021.
- [8] Lijie Fan, Kaifeng Chen, Dilip Krishnan, Dina Katabi, Phillip Isola, and Yonglong Tian. Scaling laws of synthetic images for model training... for now. In *CVPR*, 2024.
- [9] Yossi Gandelsman, Yu Sun, Xinlei Chen, and Alexei Efros. Test-time training with masked autoencoders. In *NeurIPS*, 2022.
- [10] Yaroslav Ganin and Victor Lempitsky. Unsupervised domain adaptation by backpropagation. In *ICML*, 2015.
- [11] Jin Gao, Jialing Zhang, Xihui Liu, Trevor Darrell, Evan Shelhamer, and Dequan Wang. Back to the source: Diffusion-driven adaptation to test-time corruption. In *CVPR*, 2023.
- [12] Jiayi Guo, Chaoqun Du, Jiangshan Wang, Huijuan Huang, Pengfei Wan, and Gao Huang. Assessing a single image in reference-guided image synthesis. In *AAAI*, 2022.
- [13] Jiayi Guo, Chaofei Wang, You Wu, Eric Zhang, Kai Wang, Xingqian Xu, Humphrey Shi, Gao Huang, and Shiji Song. Zero-shot generative model adaptation via image-specific prompt learning. In *CVPR*, 2023.
- [14] Jiayi Guo, Xingqian Xu, Yifan Pu, Zanlin Ni, Chaofei Wang, Manushree Vasu, Shiji Song, Gao Huang, and Humphrey Shi. Smooth diffusion: Crafting smooth latent spaces in diffusion models. In *CVPR*, 2024.
- [15] Kaiming He, Xiangyu Zhang, Shaoqing Ren, and Jian Sun. Deep residual learning for image recognition. In *CVPR*, 2016.
- [16] Dan Hendrycks and Thomas Dietterich. Benchmarking neural network robustness to common corruptions and perturbations. In *ICLR*, 2019.
- [17] Martin Heusel, Hubert Ramsauer, Thomas Unterthiner, Bernhard Nessler, and Sepp Hochreiter. Gans trained by a two time-scale update rule converge to a local nash equilibrium. In *NeurIPS*, 2017.
- [18] Jonathan Ho, Ajay Jain, and Pieter Abbeel. Denoising diffusion probabilistic models. In *NeurIPS*, 2020.
- [19] Judy Hoffman, Eric Tzeng, Taesung Park, Jun-Yan Zhu, Phillip Isola, Kate Saenko, Alexei Efros, and Trevor Darrell. Cycada: Cycle-consistent adversarial domain adaptation. In *ICML*, 2018.
- [20] Gao Huang, Zhuang Liu, Laurens Van Der Maaten, and Kilian Q Weinberger. Densely connected convolutional networks. In *CVPR*, 2017.

- [21] Jogendra Nath Kundu, Naveen Venkat, R Venkatesh Babu, et al. Universal source-free domain adaptation. In *CVPR*, 2020.
- [22] Rui Li, Qianfen Jiao, Wenming Cao, Hau-San Wong, and Si Wu. Model adaptation: Unsupervised domain adaptation without source data. In *CVPR*, 2020.
- [23] Yanghao Li, Naiyan Wang, Jianping Shi, Jiaying Liu, and Xiaodi Hou. Revisiting batch normalization for practical domain adaptation. In *ICLR Workshops*, 2017.
- [24] Zhiheng Li, Ivan Evtimov, Albert Gordo, Caner Hazirbas, Tal Hassner, Cristian Canton Ferrer, Chenliang Xu, and Mark Ibrahim. A whac-a-mole dilemma: Shortcuts come in multiples where mitigating one amplifies others. In *CVPR*, 2023.
- [25] Jian Liang, Dapeng Hu, and Jiashi Feng. Do we really need to access the source data? source hypothesis transfer for unsupervised domain adaptation. In *ICML*, 2020.
- [26] Ze Liu, Yutong Lin, Yue Cao, Han Hu, Yixuan Wei, Zheng Zhang, Stephen Lin, and Baining Guo. Swin transformer: Hierarchical vision transformer using shifted windows. In *ICCV*, 2021.
- [27] Zhuang Liu, Hanzi Mao, Chao-Yuan Wu, Christoph Feichtenhofer, Trevor Darrell, and Saining Xie. A convnet for the 2020s. In *CVPR*, 2022.
- [28] Ilya Loshchilov and Frank Hutter. Decoupled weight decay regularization. In *ICLR*, 2019.
- [29] Eric Mintun, Alexander Kirillov, and Saining Xie. On interaction between augmentations and corruptions in natural corruption robustness. In *NeurIPS*, 2021.
- [30] Arthur Moreau, Nathan Piasco, Dmzmitry Tsishkou, Bogdan Stanciulescu, and Arnaud de La Fortelle. Lens: Localization enhanced by nerf synthesis. In *CoRL*, 2022.
- [31] Weili Nie, Brandon Guo, Yujia Huang, Chaowei Xiao, Arash Vahdat, and Anima Anandkumar. Diffusion models for adversarial purification. In *ICML*, 2022.
- [32] William Peebles and Saining Xie. Scalable diffusion models with transformers. In *ICCV*, 2023.
- [33] Xingchao Peng, Baochen Sun, Karim Ali, and Kate Saenko. Learning deep object detectors from 3d models. In *ICCV*, 2015.
- [34] Mihir Prabhudesai, Tsung-Wei Ke, Alexander Cong Li, Deepak Pathak, and Katerina Fragkiadaki. Diffusion-tta: Test-time adaptation of discriminative models via generative feedback. In *NeurIPS*, 2023.
- [35] Robin Rombach, Andreas Blattmann, Dominik Lorenz, Patrick Esser, and Björn Ommer. High-resolution image synthesis with latent diffusion models. In *CVPR*, 2022.
- [36] German Ros, Laura Sellart, Joanna Materzynska, David Vazquez, and Antonio M Lopez. The synthia dataset: A large collection of synthetic images for semantic segmentation of urban scenes. In *CVPR*, 2016.
- [37] Artem Rozantsev, Vincent Lepetit, and Pascal Fua. On rendering synthetic images for training an object detector. *Computer Vision and Image Understanding*, 2015.
- [38] Shiori Sagawa, Pang Wei Koh, Tatsunori B Hashimoto, and Percy Liang. Distributionally robust neural networks for group shifts: On the importance of regularization for worst-case generalization. In *ICLR*, 2020.
- [39] Chitwan Saharia, William Chan, Saurabh Saxena, Lala Li, Jay Whang, Emily Denton, Seyed Kamyar Seyed Ghasemipour, Raphael Gontijo-Lopes, Burcu Karagol Ayan, Tim Salimans, Jonathan Ho, David J. Fleet, and Mohammad Norouzi. Photorealistic text-to-image diffusion models with deep language understanding. In *NeurIPS*, 2022.
- [40] Swami Sankaranarayanan, Yogesh Balaji, Arpit Jain, Ser Nam Lim, and Rama Chellappa. Learning from synthetic data: Addressing domain shift for semantic segmentation. In *CVPR*, 2018.
- [41] Ramprasaath R Selvaraju, Michael Cogswell, Abhishek Das, Ramakrishna Vedantam, Devi Parikh, and Dhruv Batra. Grad-cam: Visual explanations from deep networks via gradient-based localization. In *ICCV*, 2017.
- [42] Yu Sun, Xiaolong Wang, Zhuang Liu, John Miller, Alexei Efros, and Moritz Hardt. Test-time training with self-supervision for generalization under distribution shifts. In *ICML*, 2020.
- [43] Yonglong Tian, Lijie Fan, Kaifeng Chen, Dina Katabi, Dilip Krishnan, and Phillip Isola. Learning vision from models rivals learning vision from data. In *CVPR*, 2024.
- [44] Yonglong Tian, Lijie Fan, Phillip Isola, Huiwen Chang, and Dilip Krishnan. Stablerep: Synthetic images from text-to-image models make strong visual representation learners. In *NeurIPS*, 2024.
- [45] Brandon Trabucco, Kyle Doherty, Max Gurinas, and Ruslan Salakhutdinov. Effective data augmentation with diffusion models. In *ICLR*, 2024.
- [46] Yun-Yun Tsai, Fu-Chen Chen, Albert YC Chen, Junfeng Yang, Che-Chun Su, Min Sun, and Cheng-Hao Kuo. Gda: Generalized diffusion for robust test-time adaptation. *CVPR*, 2024.

- [47] Dequan Wang, Evan Shelhamer, Shaoteng Liu, Bruno Olshausen, and Trevor Darrell. Tent: Fully test-time adaptation by entropy minimization. In *ICLR*, 2021.
- [48] Qin Wang, Olga Fink, Luc Van Gool, and Dengxin Dai. Continual test-time domain adaptation. In *CVPR*, 2022.
- [49] Sheng-Yu Wang, Oliver Wang, Richard Zhang, Andrew Owens, and Alexei A Efros. Cnn-generated images are surprisingly easy to spot... for now. In *CVPR*, 2020.
- [50] Zhendong Wang, Jianmin Bao, Wengang Zhou, Weilun Wang, Hezhen Hu, Hong Chen, and Houqiang Li. Dire for diffusion-generated image detection. In *ICCV*, 2023.
- [51] Xingqian Xu, Jiayi Guo, Zhangyang Wang, Gao Huang, Irfan Essa, and Humphrey Shi. Prompt-free diffusion: Taking "text" out of text-to-image diffusion models. *arXiv:2305.16223*, 2023.
- [52] Xingqian Xu, Zhangyang Wang, Gong Zhang, Kai Wang, and Humphrey Shi. Versatile diffusion: Text, images and variations all in one diffusion model. In *ICCV*, 2023.
- [53] Lin Yen-Chen, Pete Florence, Jonathan T Barron, Tsung-Yi Lin, Alberto Rodriguez, and Phillip Isola. Nerf-supervision: Learning dense object descriptors from neural radiance fields. In *ICRA*, 2022.
- [54] Marvin Zhang, Sergey Levine, and Chelsea Finn. Memo: Test time robustness via adaptation and augmentation. In *NeurIPS*, 2022.

## A Appendix

### A.1 Synthetic Data Fine-tuning

The fine-tuning settings for our Synthetic-domain Alignment (SDA) framework are specified in Tab. 7. All results for SDA were achieved using these settings. Following DDA [11], we utilize the mmpre-train project [4] to download pretrained models and conduct fine-tuning on them.

Table 7: **Synthetic data fine-tuning settings.** We apply the same fine-tuning setting across Swin-T/B and ConvNeXt-T/B models.

Config	ResNet-50	Swin-T/B	ConvNeXt-T/B
optimizer	SGD	AdamW	AdamW
base learning rate	5e-4	2e-5	2e-5
weight decay	1e-4	1e-8	1e-8
optimizer momentum	0.9	$\beta_1, \beta_2 = 0.9, 0.999$	$\beta_1, \beta_2 = 0.9, 0.999$
batch size	512	1024	1024
training epochs	15	15	15
learning rate schedule	step decay at epoch 10, $\gamma = 0.1$	cosine decay	cosine decay
warmup epochs	None	5	5
warmup schedule	N/A	linear	linear

### A.2 Data Sensitivity Comparison

We investigate the sensitivity of different TTA methods to the amount and order of target data. For online model adaptation TTA methods, such as Tent [47], performance is robust when processing target images with large batch sizes and mixed classes and types. However, these methods exhibit significant performance degradation when faced with small batch sizes, for example, a batch size of one and streaming data with unmixed classes. In contrast, data adaptation TTA methods address this issue by processing each target image independently. Among these methods, our SDA framework demonstrates the best performance.

Table 8: **Data sensitivity comparison.** SDA maintains the insensitivity to the amount and order of target data as existing diffusion-driven TTA methods.

Method	Mixed Classes	Mixed Types	Batch Size	ResNet-50	Swin-T	ConvNeXt-T
Tent [47]	$\times$	$\times$	1 / 64	2.2 / 0.4	0.2 / 0.2	0.1 / 1.4
	$\times$	$\checkmark$	1 / 64	1.6 / 0.5	0.2 / 0.5	0.3 / 1.6
	$\checkmark$	$\times$	1 / 64	3.0 / 7.6	0.1 / 43.3	0.2 / 48.8
	$\checkmark$	$\checkmark$	1 / 64	2.3 / 3.9	0.3 / <b>44.1</b>	0.3 / <b>51.9</b>
Source				18.7	33.1	39.3
MEMO [54]				24.7	29.5	37.8
DiffPure [31]				16.8	24.8	28.8
GDA [46]	N/A		N/A	31.8	42.2	44.8
DDA [11]				29.7	40.0	44.2
SDA (Ours)				<b>32.5</b>	<b>42.5</b>	<b>47.0</b>

### A.3 Additional Detailed Comparison on ImageNet-C

We present detailed comparisons between our Synthetic-domain Alignment (SDA) framework and baseline methods for each type of corruption on ImageNet-C in Fig. 5. These comparisons were conducted using four classifiers: ResNet-50, Swin-T, ConvNeXt-T, and Swin-B. Consistent with the results shown for ConvNeXt-B in Fig. 3, SDA outperforms the baselines under most corruption types.

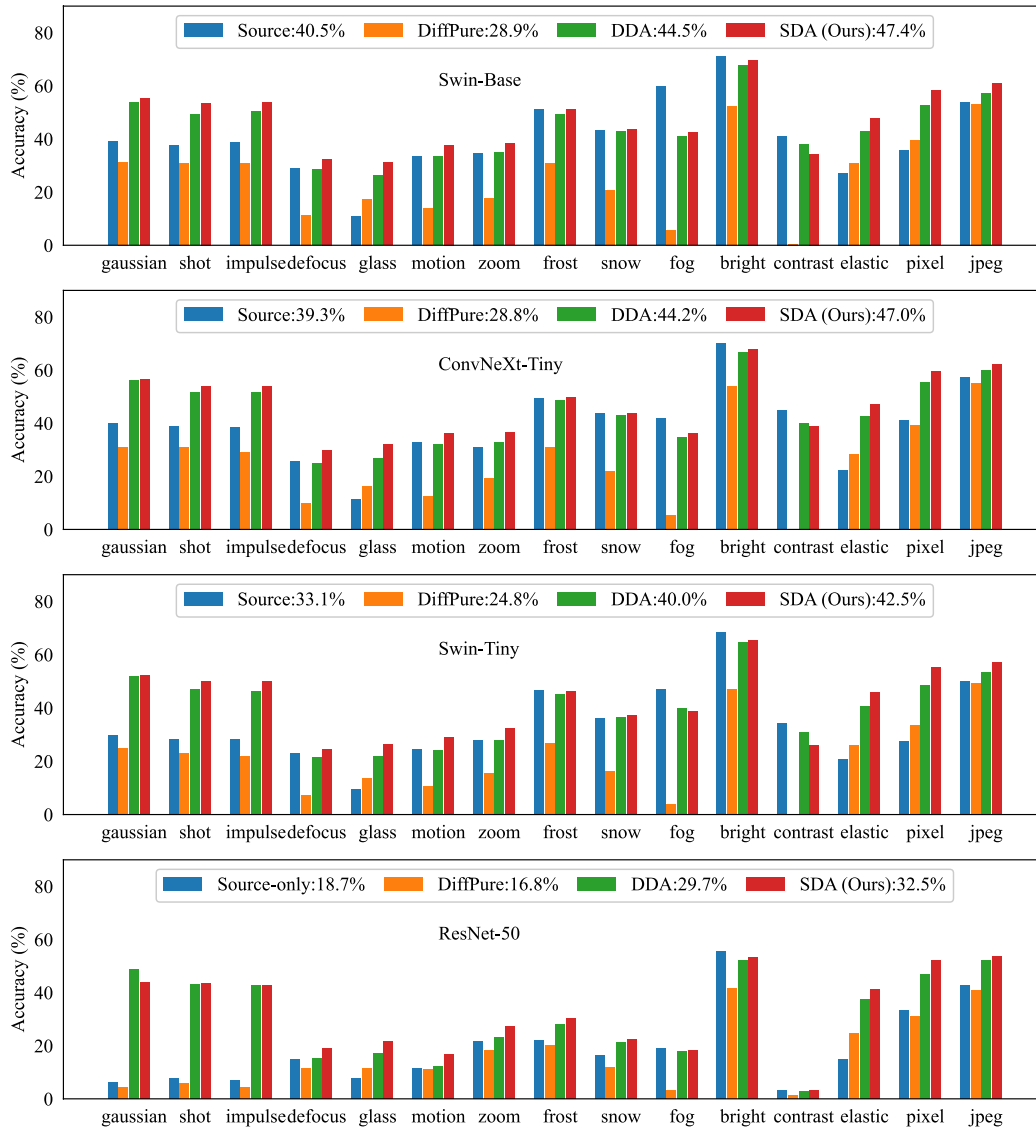


Figure 5: **Detailed comparisons of SDA and baselines under 15 corruption types on ImageNet-C.** SDA consistently surpasses the baselines across most corruption types, demonstrating the highest average accuracy. The evaluations were performed using four classifiers: Swin-B, ConvNeXt-T, Swin-T, and ResNet-50. Results for ConvNeXt-B are available in Fig. 3.

#### A.4 Additional Visualization Results

We provide additional GradCAM visualization results in Fig. 6. Consistent with our findings in Fig. 4, SDA produces activation maps and predictions that closely match those from the “source image with source model” scenario. This is mainly because SDA effectively aligns both the domains of the model and data with the synthetic domain.

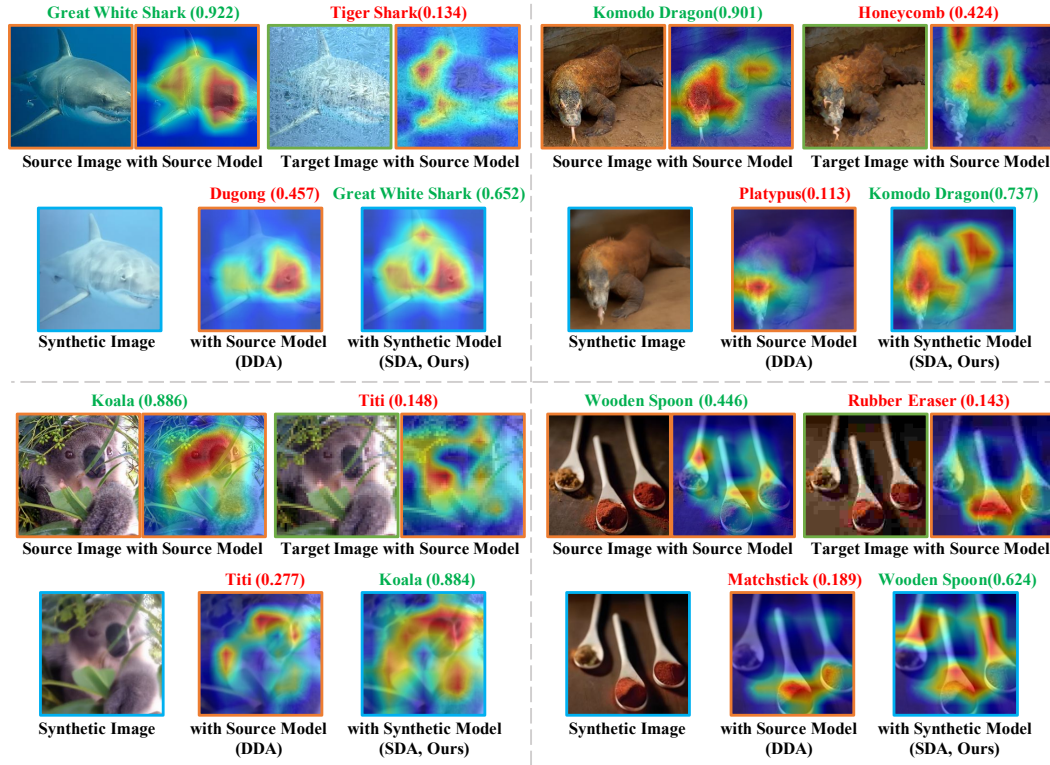


Figure 6: **Gradient-weighted Class Activation Mapping (Grad-CAM) Visualization Comparison.** The first row shows activation maps when evaluating *source* and *target* domain images using the *source* model. The second row presents activation maps when evaluating diffusion *synthetic* images using the *source* model (DDA) and our *synthetic*-domain model (SDA). The corresponding prediction classes and confidence scores are displayed above the images. Our SDA achieves alignment within the synthetic domain and, therefore, showcases activation maps and prediction results that aligns more closely with those from the “source image with source model” scenario.